Aerodynamic Simulation of A Container Ship to Evaluate Cargo Configuration Effect on Frontal Wave Loads

Article *in* China Ocean Engineering · January 2018

DOI: 10.1007/s13344-018-0021-1

CITATIONS
5

READS
469

2 authors:

Hamed Majidian
Islamic Azad University
7 PUBLICATIONS **7** CITATIONS
SEE PROFILE

Farhood Azarsina
Islamic Azad University
36 PUBLICATIONS **46** CITATIONS
SEE PROFILE

Aerodynamic Simulation of A Container Ship to Evaluate Cargo Configuration Effect on Frontal Wave Loads

Hamed Majidian[a], Farhood Azarsina[b, *]

[a] Master of Science in Ship Structures, Department of Naval Architecture, Science and Research Branch, Islamic Azad University, Tehran, Iran

[b] Assistant professor, Department of Naval Architecture, Science and Research Branch, Islamic Azad University, Tehran, Iran

Abstract

Fuel consumption has always been a matter of concern for ships propulsion. In this research we aim to develop computer models of several container ship cargo stacking configurations and discuss an optimal configuration at a constant speed front wind. The paper presents the simulation results using ANSYS CFX™ commercial software for a Post-Panamax 9000 TEU container ship. The ship is modelled in a 1:4 scale and then using unstructured mesh the wind field around it is solved. Simulation results demonstrate the influence of the container configuration on the wind load distribution. Also the numerical results are verified versus wind tunnel test data. An optimal stack configuration led to about 25% reduction in air resistance. It is proposed that in order to reduce the wind drag force and consequently reduce the fuel consumption and pollutant emissions, one should inhibit leaving empty spaces between the cargo containers and unbalanced cargo distribution over the deck. Also, it is advised to make the cargo distribution on the most forward and aftward deck areas more streamlined.

Key words: container ship, numerical simulation, wind force, cargo stacking optimization

1. Introduction

Generally, in calm sea state, wind resistance comprises 3% to 5% of the total ship resistance (Moonesun, 2010) but in container ship which possessed large windage area, wind resistance comprises significant amount of total resistance about 2% to 10% (Minsaas and Steen, 2008). The wind forces on a ship generally influence the ship by increasing the induced resistance. The longitudinal force generally constitutes the largest part of the total wind induced resistance. The transverse force causes yaw, drift and deviation of vessel from the desired course, which can cause the added resistance in two ways: (i) the ship's heading will not be aligned with the steered course which leads to great resistance; (ii) the drift must be compensated for, which means that the rudder angle must be increased repeatedly. Increasing the rudder angle will also increase resistance; this leads to wearing out of steering gear system and increase of fuel consumption and gas emission, especially during extended periods of execution. Magnitude of resistance compared with the longitudinal force is discussed by Andersson (1978) and van Berlekom (1981). According to Andersson (1978) the induced resistance from the increased rudder angle plays an insignificant role, while according to van Berlekom (1981) it can be of the same magnitude as the longitudinal force for stronger winds. Generally, the longitudinal force is of greatest importance for the propulsion resistance. Its share in the total resistance has been discussed by van Berlekom (1981) and Aage (1968). According to van Berlekom (1981), the wave and wind resistance are of the same magnitude. However, Aage (1968) stated that the wind resistance rarely contributed more than 10% of the total resistance.

For the first time it was concluded by Blendermann (1997) that the wind forces are influenced by container stacking configuration. Blendermann (1997) stated that the uneven bay heights increase the wind resistance. A ship with randomly stacked containers on deck compared with a fully stacked ship experiences significantly higher longitudinal force, smaller transverse force, smaller roll moment, and smaller yaw moment (Blendermann, 1997).

In Andersson (1978), test results for the longitudinal force is summarized as (i) less significant effect between empty ship and a ship which only carries containers on the aft deck; (ii) a significant effect due to container configuration on the fore deck; (iii) irregularities such as many empty bays has a significant effect of up to 70%–100% increased force compared with the fully stacked reference ship; (iv) full load on the fore deck and streamlining of the aft deck is most favorable of the 19 tested configurations.

Andersen (2012a, 2012b) presented experiments with streamlined versus uneven container configurations. Wind tunnel test model was developed by increasing the number of stacking configuration from 6 to 16, while the longitudinal force and yaw moment were investigated. Minimum amount of longitudinal forces were experienced when containers in aft and forward deck were streamlined. In the streamlined condition, reduction of yaw moment was experienced in fore deck while the maximum yaw moment was experienced for aft deck configuration. In full stack configuration, the longitudinal force was extensively increased.

* Corresponding author. E-mail: F.Azarsina@srbiau.ac.ir

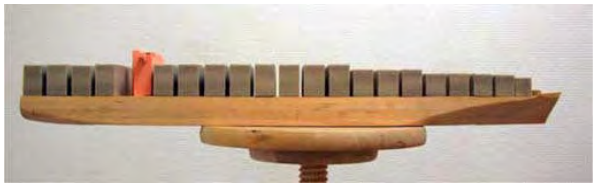

Fig. 1. Full stack configuration of Post-Panamax container ship test model in wind tunnel (Andersen, 2012b).

Hassan et al. (2012) investigated the effect of container configuration on wind resistance of container ship in association with the longitudinal and lateral forces along with pressure contours and velocity streamlines through computational fluid dynamics approach. Furthermore, 14 different stacking configurations were investigated from 0° to 90° wind directions. Finally, the alteration of wind resistance force and its effect on fuel consumption and gas emission was investigated (Hassan et al., 2012). They simulated the natural sea conditions; in other words, simulation domain and boundary conditions were selected so as to meet the natural sea conditions for a container vessel. A 2800 TEU container ship of 221.65 m in length overall was modelled. Steady state condition with three million mesh cells and $k-\epsilon$ turbulence model were considered for the solver set-up. The study, however, lacked any extensive verification with experimental data. Validation of numerical result was confined to the customary empirical formula.

To analyze aerodynamic performance of a Post-Panamax container ship with different container stacking configuration models on deck, by means of CFD along with comparison of the achieved results against experimental data, and to analyze wind force under alteration of container stacking configurations are the most important goals of the present study. In addition, to check the challenges of a numerical investigation of the above subject, such as the flow turbulence pattern and its influence on wind force, comprise subsidiary targets of the present study. Pressure contours and velocity streamlines at critical locations as the containers loading vary on the deck are investigated.

2. Computational fluid dynamics

In this study, CFD employed for computation of the mass conservation, momentum and energy equation around the vessel's body. By splitting up (discretizing) the nominated area for analysis into the smaller parts and applying of the boundary conditions over boundary nodes with exerting approximation, a linear equation system is obtained to solve which, the velocity and pressure field will be attained over the assigned domain. To this point, ANSYS CFX™ is used which is recognized as the one of the most powerful fluid flow analysis packages. A finite volume method (FVM) is used by the software (ANSYS, 2009).

An exclusive feature of the software is to use one unit for all steps of the simulation process including the geometry and grid generation, physical definition of the model state, solver and post solver process. Diverse types of grid are producible by the software including the triangular and tetrahedron mesh element for 2D geometries and tetrahedron, hexahedron, pyramidal and wedge for 3D geometries. The present study employes a 3D grid. Also the software provides the ability of the grid size alteration in boundaries and the required area of geometries for the operator. This feature causes precise optimization of the vortex and eddies region i.e. inner part of the boundary layers.

2.1 Assumptions

Owing to the high amount of computation, the following simplifying assumptions have been considered in this study.

(1) Only the above waterline ship's body has been inspected for the effect of wind analysis.
(2) The fluid flow is 3D and for turbulence effect determination, $k-\omega$ and SST model have been used.
(3) The ship's geometry is symmetrical in length therefore the symmetry condition has been considered and the demi-body of the model is inspected.
(4) The ship is supposed to be fixed with zero heel and trim.
(5) Owing to the computing conservation, the nearest practical scale of ship has been adopted for simulation.
(6) Wind has transient nature but with respect to the studied forces, it has been supposed under the steady state condition.

2.2 Analysis method

Excessive dimension of the solving domain, particularly in wind tunnel simulation that lateral boundaries negatively affect the solution condition is very important. On the other hand, by considering the excessive domain, it intensively increases the calculation grid and eventually increases the solving time. Therefore, attaining an appropriate computational optimal domain requires trials and experience. In the present study, the optimal computational domain has been considered with respect to test space dimensions (Table 1) (Andersen, 2012a, 2012b). To prevent software computational error and prepare proper conditions for software solver, the prototype domain was scaled one to four. Incidentally, in order to decrease the volume of calculation, noting a negligible effect of over-extending domain cross-section on final results, the width and height of the domain were kept to the minimum. So regarding the above and frugality in calculation time, the dimensions of

domain has been selected according to Table 2. Whereas the limitation of boundary layers on the model body in wind tunnel does not exist in a computer model, so the length of domain has been extended long enough.

Table 1 Principal dimension of vessel

Prototype vessel (Andersen, 2012b)	
Length over all	340 m
Length between perpendiculars	320 m
Beam	45 m
Depth	27.2 m
Draft	15 m
Block coefficient	0.674
Loading capacity	9000 TEU

Table 2 Domain specification

Domain dimensions in experimental test (Andersen, 2012b)			
Prototype domain dimension		Model ship dimensions	
Length	260 cm	Length	75 cm
Width	100 cm	Width	10 cm
Height	70 cm	Height	11 cm
Domain dimensions in numerical simulation			
Scaled domain		Ship	
Length	440 m	Length	85 m
Width	40 m	Width	11.25 m
Height	50 m	Height	12.4 m

2.3 Simulation of Post-Panamax container ship

For wind force study on Post-Panamax container ship with respect to the different stacking configuration on deck, ship's body above waterline, superstructure, aft and fore deck and finally the loaded containers on deck have been simulated; 40 feet container size were used (Shipsbusiness, 2016). As it is illustrated in Fig. 2, a right-handed Cartesian coordinate system is used and then fixed across the intersection of base line passing through deck and an imaginary line passing athwartship through deck over $L_{PP}/6$. The axis direction has been adopted from ITTC (1993). Moreover, the drag force assumed in positive direction of X axis which means the angle between ship advance and the wind flow direction was 180°. Incidentally, it must be noted for domain meshing due to the complication of ship's geometry, unstructured mesh is chosen that extensively improves the precision of analysis results. Density of mesh in different parts is adjusted according to the simulation importance (Fig. 3). For this purpose, the mesh density for surface parts of vessel's hull and containers which have significant importance in equation solving, are selected in the range of 0.1 m. Mesh density inside boundary layers was up to five times inflated and in regions of high pressure exposure, particularly at the outer body of ship hull and containers, the mesh density was intensively increased (see Fig. 4). For decreasing the volume of computation, moving from the ship's hull toward the domain's wall, the density of mesh decreases respectively to the mesh size of 0.5 m. The total number of seven million meshes in two million nodes has been computed over solving domain which has proved the results more reliable. It must be noted that the gaps of bays were assumed to be 1.0 m.

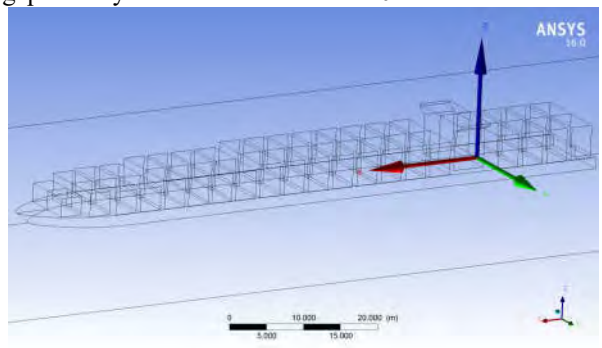

Fig. 2. Ship simulation sample in CFX software and indication of the coordinate system.

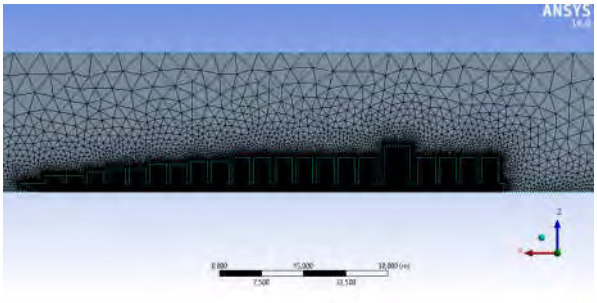

Fig. 3. Grid indication around the ship and domain.

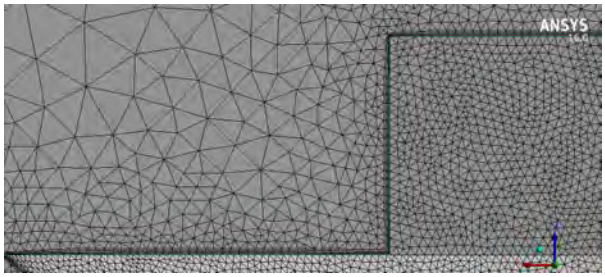

Fig. 4. Growth of grid density on the surface of the ship and containers.

2.4 Boundary condition

The aim of boundary condition in computational fluid dynamics is to converge the discretized equations for solving the specified framework in accordance with the defined flow specification around the computational domain boundaries.

For this purpose, the boundary condition of the case is to choose the wind velocity inlet profile assigned as the inlet condition (Fig. 5). For simulation relative to the real condition, the wind speed has been considered 12.85 m/s equivalent to 25 knot (Force 6 of beafurt scale). The wind speed of experimental test in wind tunnel was 45 m/s equivalent to 2200.000 Reynolds number (Andersen, 2012b). For comparison of numerical and test results non-dimensional drag force is employed. To prevent a reverse flow, the outlet boundary is considered of the pressure outlet where the magnitude of the pressure is zero. Application of the pressure outlet boundary condition, in simulations that a reverse flow occurs during iterations, results in a proper convergence rate. Owing to the symmetry of ship's geometry in order to reduce the computational efforts, the symmetry condition through the entire domain is considered with respect to *XZ* plane.

Wall boundary condition is applied where the fluid is surrounded by solid. Two-phase fluid investigation was not the subject of the present study. Hence, the sea surface is assigned as a fixed wall resembling conditions of the wind tunnel boundary condition as no-slip wall. In reality, however, the sea surface will have a surface velocity and wave elevation.

Grid density grew up due to the importance of the area where wind strikes the ship surface. However the far field wall considered the free slip wall as it was so far from the flow field and the equation solving is almost affectless there. Consideration of $y+$ on walls supports the flow contribution by reduction of computations. For lateral walls of the domain, this boundary condition has been chosen due to the symmetrical plan which is assumed as a free slip wall too.

It must be noted that the computational domain was considered large enough to minimize the effect of the lateral boundaries on vessel.

2.5 Convergence of results

Aim to approaching fine range of convergence, respect to software and hardware performance, 10 cycle of iteration minimum and 50 cycle of iteration maximum is considered which has been stopped when the difference between two successive RMS become less than 0.0001 that determining the convergence range which has been shown in Fig. 6.

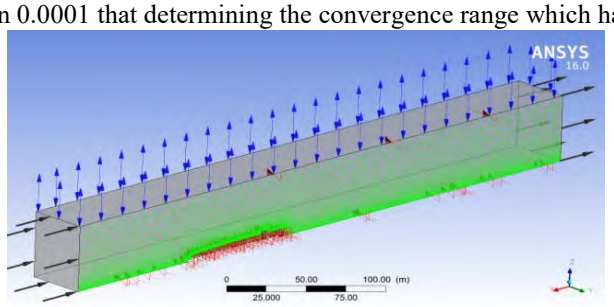

Fig. 5. indication of domain and boundary condition.

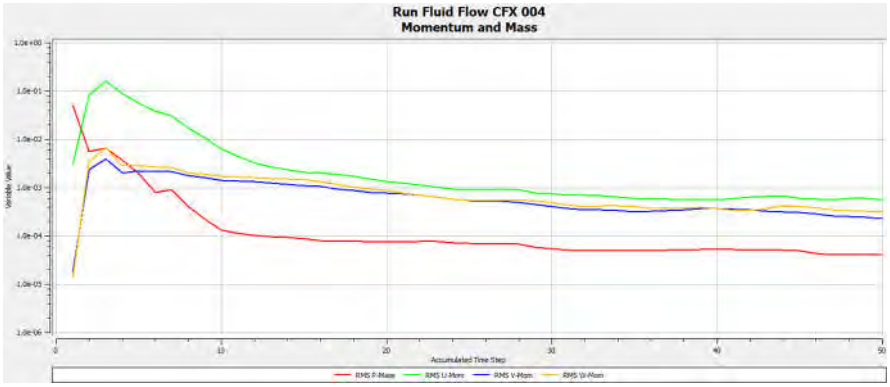

Fig. 6. Convergence of residuals in numerical solution.

2.6 Non-dimensional coefficients

The measured forces and moments are post-processed into non-dimensional coefficients to make the results independent of wind velocity and ship size. The results are normalized using the flow velocity wind profile, U, the density of the air, ρ, and the ship's length between the perpendiculars (L_{pp}) in a suitable exponent:

$$X\& = \frac{X}{1/2 \cdot \rho U^2 L_{PP}^2}. \quad (1)$$

The description of coefficients are convenient if different configurations of the same ship are to be compared because they are normalized using L_{pp}.

3. Container configurations

Ten different container stacking configurations are investigated.Stacking details are shown in Appendix 1 of the present study. Stacking configurations are divided to three categories generally. The first category includes systematic configuration, the second category includes the streamlined, and the third group includes random stacking configuration.

Of course many considerations are taken into account when loading containers on board of a ship (IMO, 2012; DNV, 2001). Some are:

- Reefer containers must be placed where the power supply for the refrigeration is located.
- Hazardous goods containers have designated locations.
- Containers are loaded for unloading in the right order at different ports of call.
- Heel, trim and stability are taken into consideration when loading the ship.
- The line of sight from the bridge must be 500 m or two ship lengths whichever are smaller, i.e. it must be possible to see the sea surface from the bridge 500 m in front of the ship, which dictates how high the containers in front of the bridge can be stacked (IMO, 2012). Furthermore stated by class that the view of the sea surface from the coning position shall not be obscured by more than two ship lengths, or 500 m, whichever are less, forward of the bow to 10° on either side under all condition of draught, trim and deck cargo (DNV, 2001).

For 0° wind blowing angle of attack which could be assumed as the head wind or air resistance against ship motion, wind counters and wind velocity passing through the model have been investigated at different container configurations. Fluid flow separation and vortex contribution around the container ship with diverse stacking configurations are a remarkable part of the present research.

4. Results for container ship's aerodynamics investigation

In the following, due to limitation exposed by page numbers of the present study only the loading condition No. 1, 4, 7 and 10 (According to Appendix 1) are explained.

4.1 Full stack loading

Deck has been loaded by maximum container stacking capacity. It is distinctively shown in Fig. 7 that the maximum amount of pressure contour is experienced in the forward part of ship's body where the wind profile impacted to ship's body. Over the last bay of containers in debut, the pressure particularly increases on the upper tier corners. Note that bays are numbered from ship aft to fore. As the exposed cross section is directly impacted by wind, the maximum pressure is experienced in this area. Here, the minimum wind speed would be expected. This does not mean wind losing power, though, and after retrieving energy, pressure increases along the ship's length. The minimum pressure occurs on the top of container

tiers surface where wind velocity increases as shown in Fig. 8. It is observable that the wind velocity strongly decreases after passing over the ship astern and the largest vortex is contributed. Other than that, the homogenous shape of container layout through stacked bays prevented any contribution of vortex between stacked bays. This is advantageous for drag force reduction.

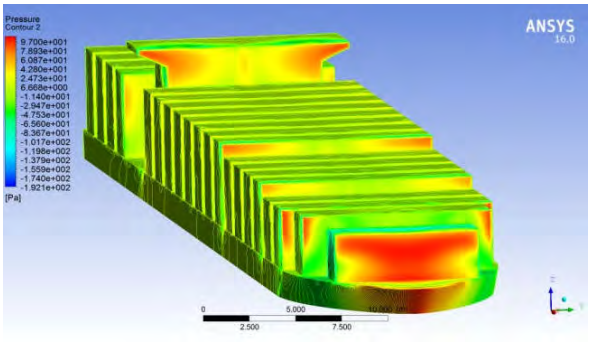

Fig. 7. Pressure contour in full stack loading condition.

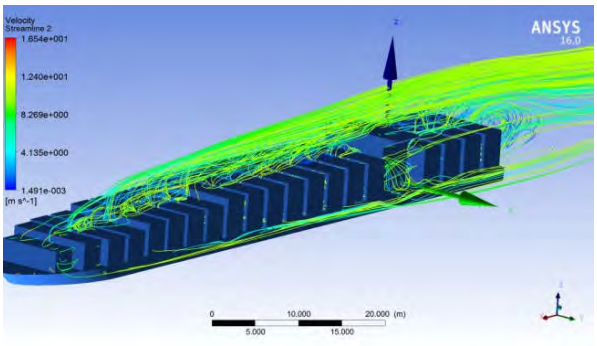

Fig. 8. Indication of velocity streamlines over the lengths of bays.

4.2 Streamlined loading through entire deck

Regarding to gradual increase of containers tiers height through bays, wind pressure is gently distributed over all bays at fore deck which possess the minimum spot pressure over all bays in comparison with other stacking configuration (see Fig. 9).

Pressure decreased through bays toward superstructure that could signify the wind pressure gradually increased along the bays (see Fig. 10).

Gradual decrease of container bays from superstructure toward astern prevents the generation of vortex and eddy current in this area which leads to attaining optimum aerodynamic shape of configuration.

The minimum flow turbulence and vortex contribution is experienced in this configuration. Owing to gradual reduction of tiers height toward forward of vessel, wind flow velocity does not slow down until the middle bays over fore deck.

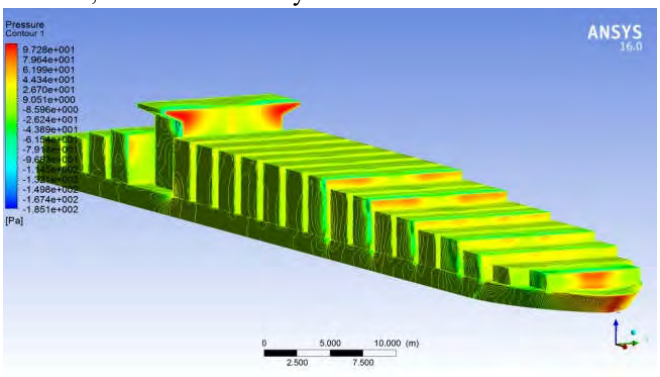

Fig. 9. Indication of pressure contour in a streamlined configuration in fore and far deck.

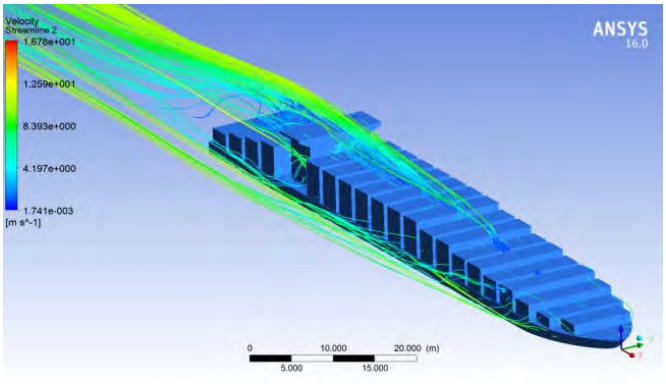

Fig. 10. Indication of streamlines over deck.

Late flow separation over mid bays is very effective in drag force reduction. In addition, the shape of superstructure in aft bays in conjunction with a stern, effectively minimized the formation of large vortices. Velocity reduction in wake is also minimized. Streamlined configuration is most favorable of aerodynamic loading condition.

4.3 Random stacking with maximum seven containers in height

In this configuration, multiple changes in bay heights along the ship length cause the added exposed cross sections which eventually lead to the growth of high pressure region in front of container bays. These high pressure regions are especially observed in the top tier corners which are directly exposed to wind flow around ship's body (see Fig. 11). Vortex formation is observable at locations where bay heights change (see Fig. 12). Whereas the loading configuration is non-homogenous, disordered wind velocity alteration occurs between bays, which leads to vortex formation between bays that has great effect on the increasing drag force. The empty spaces between bays result in the air getting enough space to regain its energy before hitting the next bay and thereby increase the resistance. Several random stacking configurations (according to Appendix 1) show similar trends in velocity and pressure behavior.

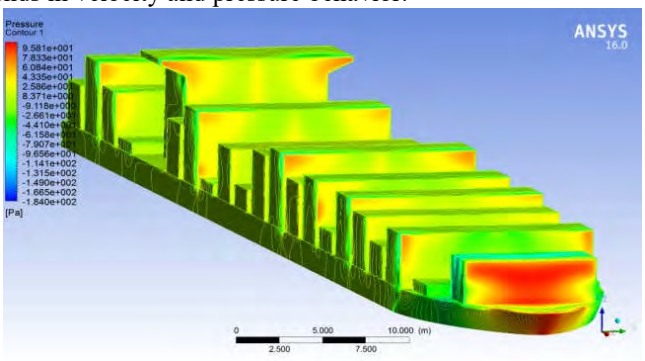

Fig. 11. Random stacking with the maximum seven containers in height.

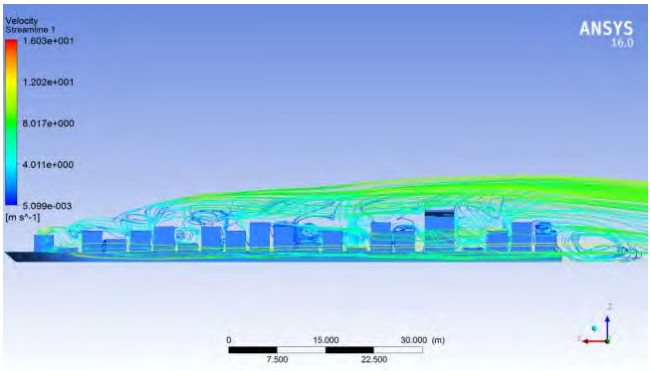

Fig. 12. Indication of streamlines passing over bays.

4.4 Pyramid stacking configuration with one container less in each bay on each side

As shown in Fig. 13, elimination of one container from the outer side of each bays has no significant effect on pressure contours. However, the area that is exposed to free wind flow on outer bays is partially reduced, therefore the drag force is reduced.

The maximum pressure is observable at ship stem and the vicinity area over water surface.

Large magnitude of ship forward cross sectional area intensifies the turbulence of wind flow that is traced in numerical solution outputs as sudden increase in drag amount (Fig. 15).

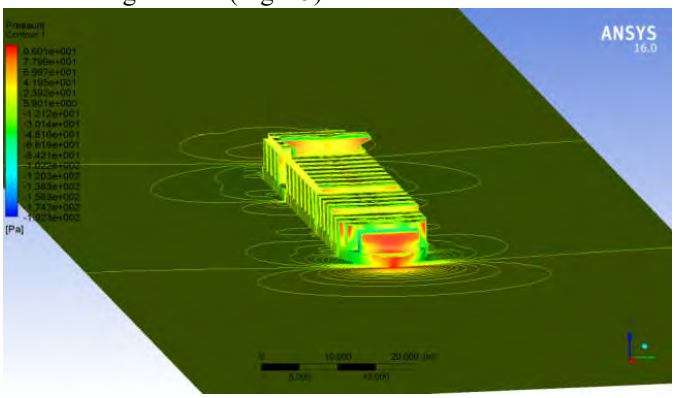

Fig. 13. Pyramid stacking with 98.2% loading capacity.

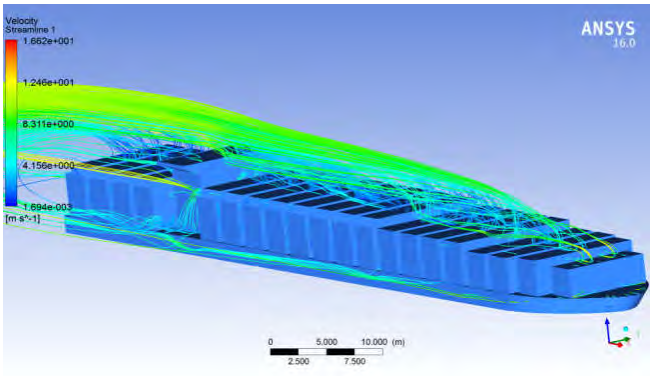

Fig. 14. Indication of streamlines passing over bays.

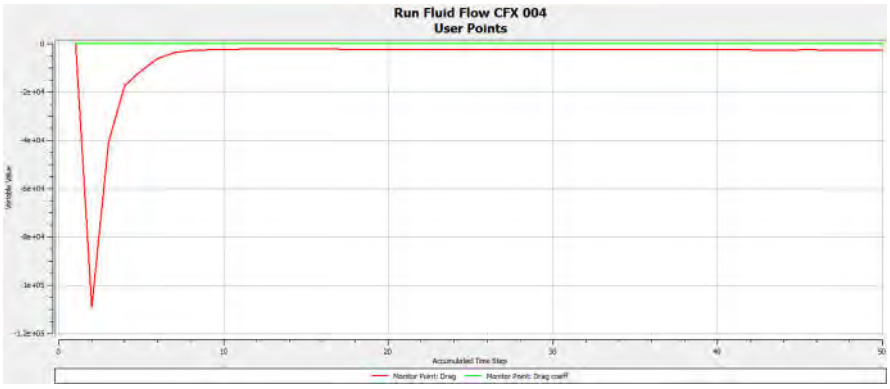

Fig. 15. Sudden increase in drag force when the wind flow impacts the forward cross section of containers at early solution time steps.

In the next part numerical results are compared versus wind tunnel experimental results in order to determine the precision of numerical method.

5. Aerodynamic drag force results

For numerical approach a Core i7 quad core CPU with 8GB Ram system has been employed. The run time of the system for grid generation was about 45 minutes and for the process about 120 minutes for each configuration.

5.1 Verification of results

A container ship similar to the one which was employed in wind tunnel test (Andersen, 2012b) was used for numerical simulation. The non-dimensional numerical results are compared with the wind tunnel test results. The blockage correction is ignored for simulation (Maciejewski and Osmólski, 2002). Achieved results have been adopted for 0° wind angle of attack (head wind) in order to compare the results in certain situation. The results of CFD solution of 5266.2 N drag force for full stack condition has been attained. Normalized drag force is 0.0084 (non-dimensional). Whilst the obtained non-dimensional drag force for the same configuration of experimental test is 0.01 which implies the reliability of the achieved numerical results.

On the other hand, results by CFD method depicted approximately the same difference for other stacking configurations. Moreover the CFD results show the same relative magnitude compared with experimental results. Also, results for different stacking configurations are presented in the diagram of Fig. 16 which shows a rational order.

In order to verify the precision in numerical results, drag coefficients for each configuration are compared with the normal drag coefficient of container ship which exists between 0.55 to 0.8 (Minsaas and Steen, 2008). While the simulations were performed for half of model, the results were doubled and presented in Fig. 17. Generally, the differences between the numerical and wind tunnel test results are about 20% which imply the reliability of the method.

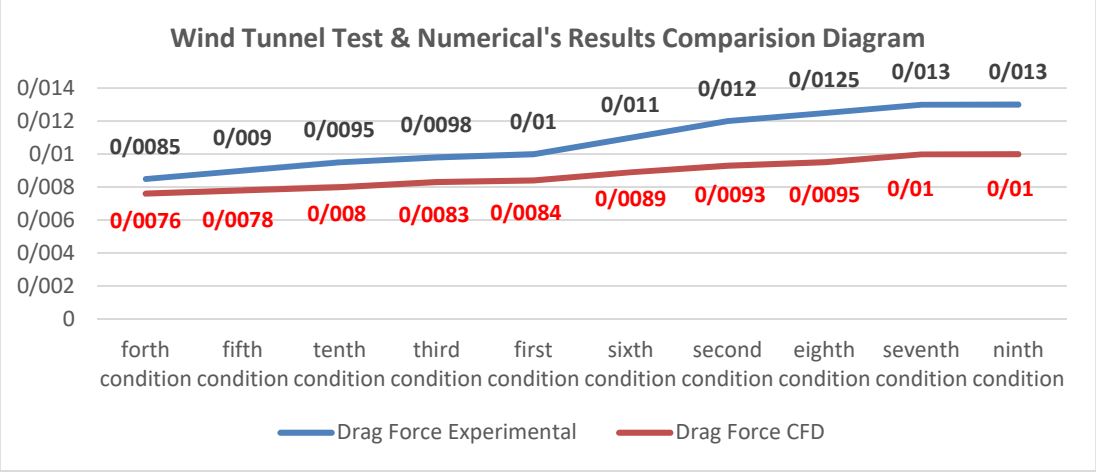

Fig. 16. CFD approach results versus wind tunnel test results of Andersen (2012b).

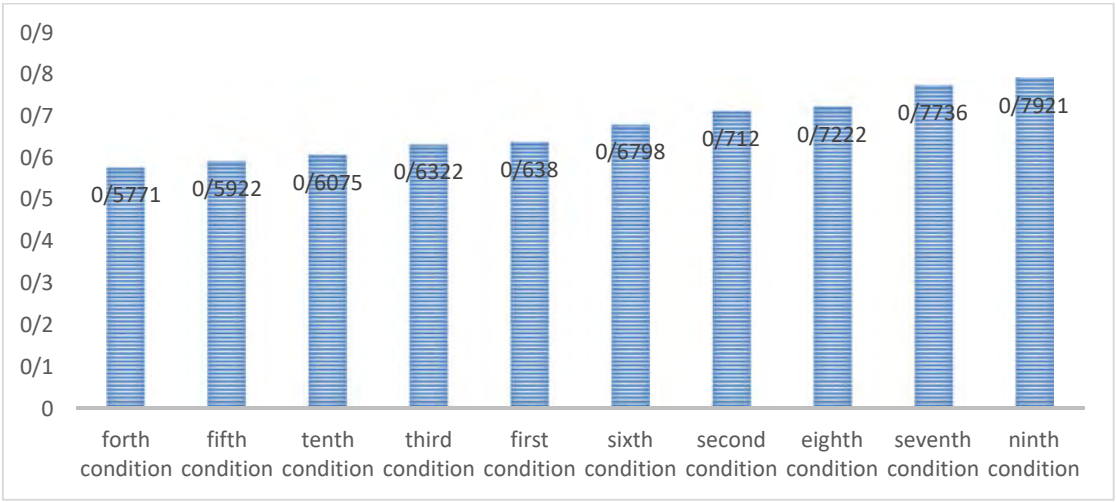

Fig. 17. Drag coefficient diagram resulted by CFD approach.

Wind drag force may also be calculated using class rules such as DNV and ABS (Hsu, 1984). The typical equation is in the following form:

$$R_{\text{wind}} = \frac{1}{2}\rho V_{\text{yt}}^2 C A \sin\alpha\,, \qquad (2)$$

where V_{yt} is the average wind speed above sea surface, C is the shape factor, A is the frontal surface area in square meters, and α is the wind angle of incidence. Inserting the respective values of 1.185 kg/m^3 for air density, 12.85 for wind speed, 84.7 m^2 for frontal area in a full stack condition (configuration #1 in Appendix 1), and also assuming a shape factor of unity, results in a wind force of 8286.6 N while the simulated value is 5266.2 N for full stack condition. This suggests that a unity

shape factor for the hull and cargo overpredicts the wind force. Instead a value of about C=0.65 can precisely correct the formula. In the case of streamlined configurations, although the frontal area to be used in Eq. (2) for seven tiers cargo is the same as a full stack, the shape factor must be further reduced. With this additional check the numerical results are verified and the CFD performance indicates well conformity.

5.2 Effect of wind velocity on drag force

Wind speed is defined as input and drag coefficient as output for full stack configuration. Results are shown in Table 3. Different speeds were selected from beafurt scale. Respectively sea force of 4, 5, 6, 7 and 8 were selected. Air density is considered 1.185 kg/m^3 and L_{pp} assumed 80 m. The results are non-dimensionalized by Eq. (1) and presented in Fig. 18.

Table 3 Numerical results for different wind velocities

Beafurt scale	Wind velocity (m/s)	Drag force (N)	Drag coefficient
4	6.5	1356.9	0.642
5	9.5	2883.8	0.639
6	12.85	5266.2	0.638
7	15	7147.4	0.635
8	19	11469.8	0.635

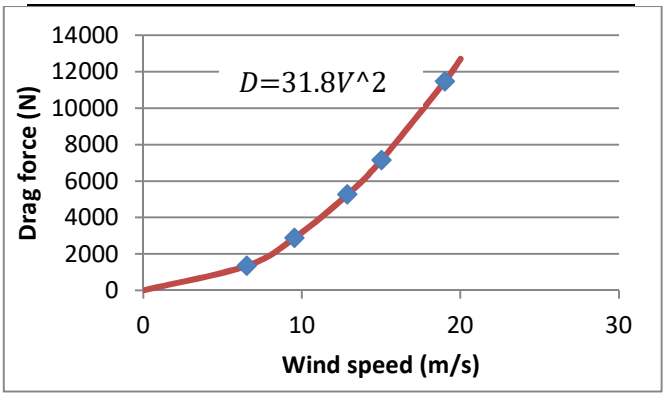

Fig. 18. Drag force diagram for different velocities.

5.3 Summary of results

In comparison to drag force in streamlined stacking condition, a full stack condition increased drag force by 9.5%, a deck with empty bays 18.2%, and a random stacking configuration 24% increase.

Difference of drag force between full streamlined stacking configuration versus full stacking in aft deck, while streamlined stacking in fore deck, was 2.6% increase. Also the difference of drag force between random full stacking on aft deck versus random stacking with maximum five containers in height was 5%.

In ten investigated stacking configurations, the difference of drag force between the fully streamlined stacking and full stack condition (which supposed as reference condition) was 10%.

Moreover, the difference of drag force between the fully streamlined stacking configuration (which supposed as optimum condition) and fore deck streamline and aft deck full load was 2.6% which indicates the minimum difference among all the stacking configurations with optimum condition. Also it was 5% with pyramid stacking condition. These three loading configurations are favorable stacking due to the drag force reduction (see Table 4).

Table 4 Percentage increase in drag force due to different stacking configurations

Optimum stacking for drag reduction	
Fully streamlined stacking in comparison with	Drag force percentage increase
Full stack	10
Aft deck full stack fore deck streamline	2.6
Pyramid stacking	5
Unfavorable stacking for drag reduction	
Fully streamlined stacking in comparison with	Drag force percentage increase
Random stacking five containers in height	24
Random stacking seven containers in height	19

In this way the difference of drag force between fully streamlined configuration and random stacking with five containers in height was 24% and with random stacking with seven containers in height was 19% that implies the random stacking configurations are unfavorable stacking conditions due to the drag force reduction.

Difference of fully streamlined stacking with even bays empty was 14.6% and with randomness was 24% that implies as far as possible for loading the even container stacking in height is more effective than random stacking configuration for drag force reduction (see Table 5).

Table 5 Effect of stacking height and randomness contrast

Optimum stacking for drag reduction	
Fully streamlined stack in comparison with	Drag force percentage increase
Even bays empty	14.6
Random stacking 5 containers in height	24

6. Conclusions

A Post-Panamax container ship has been simulated in ANSYS CFX™ software in order to compare the achieved longitudinal force values with wind tunnel test results as the container stacking configuration varies over deck. Generally, the effect of container stacking configuration on drag force at head winds could be concluded as the following results.

Every change of stacked configuration on deck has direct influence on drag force. The drag force depends on both the ship cross sectional area, as well as the amount of ship's longitudinal surface over which wind passes. In fact, the latter has a more significant effect.

From summary of results, it could be concluded that every empty bay caused additional flow turbulence. Thus, as far as possible loading with empty bay must be avoided during ship voyage due to the effect of random stacking and empty bays on drag force increase. It is revealed that change of stacking configuration on aft deck led to the increase of drag force. Regarding to the attained results the fore deck stacking configuration does have the main significant role in change of drag force, while, the aft deck stacking configuration also alters the drag force. Fore and aft deck streamlined is the optimum stacking configuration. Fully streamlined, aft deck full stack while fore deck streamlined, and pyramid stacking condition are three favorable stacking configurations for the drag force reduction.

As a general instruction for drag force reduction, any unevenness and random stacking must be avoided during loading of container on deck. Also during seakeeping, the same configuration instruction could be advantageous due to the resistance reduction.

It is proposed that in order to reduce the wind drag force and consequently reduce the fuel consumption and pollutant emissions, inhibit leaving empty spaces between the cargo containers and to prohibit unbalanced cargo distribution over deck. Also, it is advised to make the cargo distribution on the most forward and aftward deck areas more streamlined.

References

Aage, C., 1968. *Wind Power in Ships*,Technical University of Denmark.

Andersson, G.O., 1978. *Untersuchung der Fahrtverluste durch Wind und Seegang bei einem schnellen Einschrauben-Containerschiff*, Bundesministerium für Forschung und Technologie, Meerestechnik. (请核对文献类型)

Andersen, I.M.V., 2012a. *Wind Forces on Container Ships*, Mercator. (请补充出版地且核对文献类型)

Andersen, I.M.V., 2012b. Wind-tunnel investigation of wind loads on a post-panamax container ship as a function of the container configuration on deck, *International Marine Design Conference 2012*, Glasgow. (请补充出版社)

ANSYS, 2009. *ANSYSCFX Solver Theory Guide*, release 12.1. (请补充出版信息)

Blendermann, W., 1997. *Measurement of Wind Load on Two Container Vessels in the Real State of Charge in the Wind Tunnel*,Institute of Naval Architecture, University of Hamburg.

DNV, 2001. *Rules for Classification of Ships Newbuildings Machinery and Systems Main Class*, *Part 4*, *Chapter 11 Safety of Navigation*, Det Norske Veritas.

Hassan, K., White, M.F. and Ciortan, C., 2012. Effect of container stack arrangementson the power optimization of a container ship. *Journal of Ship Production and Design*, 28(1), 10–19.

Hsu, T.H., 1984. *Applied Offshore Structural Engineering*,Gulf Publishing Company,Houston.

IMO, 2012. *Safety of Life at Sea Convention* (*SOLAS*), London Maritime Arbiters Association.

ITTC, 1993. ITTC symbols and terminology list, version 1993, *International Towing Tank Conference*, Versuchsanstalt für Wasserbau und Schiffbau, Berlin. (请核对文献类型与作者)

Maciejewski, M. and Osmólski, W., 2002. Numerical simulation of the blockage effect in wind-tunnels, in: Verbraeck, A., Krug, W.(eds.), *Proceedings of the 14th European Simulation Symposium*. (请补充出版信息)

Minsaas, K. and Steen, S., 2008. *Ship Resistance*: *Proceedings and Lecture Notes*, Norwegian University of Science and Technology, Norway.

Moonesun, M., 2010. *Handbook of Naval Architect and Marine Engineering*, Kannon Pajohesh Publication, Tehran. (in Persian)

Shipsbusiness, 2016. *Container Ship Operations*. shipsbusiness.com[2016-12].

van Berlekom, W.B., 1981. *Wind Forces on Modern Ship Forms-Effects on Performance*, RINA, London.

Appendix 1: Information of 10 studied container stacking configurations

No.	Stacking condition	Bays configuration	Tiers configuration	Loading capacity (%)
1	Full stack	1–13	7	100
		13–15	6	
		15–19	5	
		20	4	
2	All bays 1 container	1–20	1	15.8
3	Even height	1–20	5	78.25
4	Full streamline	1	3	83.1
		2	4	
		3	5	
		4	6	
		5–11	7	
		12–13	6	
		14–15	5	
		16–17	4	
		18	3	
		19–20	2	
5	Fore deck streamline aft deck full stack	1–11	7	91.1
		11–12	6	
		13–14	5	
		15–16	4	
		17–18	3	
		19–20	2	
6	Even bays empty	1–12	7	51.1
		13–16	6	
		17–20	5	
7	Random	1–20	Max. 7	68.9
8	Fore deck random aft deck full stack	1–4	7	77.8
		5–20	Max. 7	
9	Random	1–20	Max. 5	42.6
10	Pyramid shape	٧1–12	7	98.2
		13–15	6	
		16–19	5	
		20	4	